nature materials

ARTICLES

https://doi.org/10.1038/s41563-021-01073-5

Check for updates

Confining isolated chromophores for highly efficient blue phosphorescence

Wenpeng Ye[1,8], Huili Ma[1,8], Huifang Shi[1,8], He Wang[1], Anqi Lv[1], Lifang Bian[1], Meng Zhang[1], Chaoqun Ma[1], Kun Ling[1], Mingxing Gu[1], Yufeng Mao[1], Xiaokang Yao[1], Chaofeng Gao[1], Kang Shen[1], Wenyong Jia[1], Jiahuan Zhi[1], Suzhi Cai[1], Zhicheng Song[1], Jingjie Li[1], Yanyun Zhang[1], Song Lu[1], Kun Liu[1], Chaomin Dong[1], Qian Wang[1], Yudong Zhou[1], Wei Yao[1], Yujian Zhang[2], Hongmei Zhang[3], Zaiyong Zhang[4], Xiaochun Hang[1], Zhongfu An[1]✉, Xiaogang Liu[5,6]✉ and Wei Huang[1,3,7]✉

High-efficiency blue phosphorescence emission is essential for organic optoelectronic applications. However, synthesizing heavy-atom-free organic systems having high triplet energy levels and suppressed non-radiative transitions—key requirements for efficient blue phosphorescence—has proved difficult. Here we demonstrate a simple chemical strategy for achieving high-performance blue phosphors, based on confining isolated chromophores in ionic crystals. Formation of high-density ionic bonds between the cations of ionic crystals and the carboxylic acid groups of the chromophores leads to a segregated molecular arrangement with negligible inter-chromophore interactions. We show that tunable phosphorescence from blue to deep blue with a maximum phosphorescence efficiency of 96.5% can be achieved by varying the charged chromophores and their counterions. Moreover, these phosphorescent materials enable rapid, high-throughput data encryption, fingerprint identification and afterglow display. This work will facilitate the design of high-efficiency blue organic phosphors and extend the domain of organic phosphorescence to new applications.

Blue-emitting phosphors have drawn considerable attention due to potential applications in display, lighting, biomedicine and optical communication[1–5]. For instance, blue light is the core component of white emission for solid-state lighting and full-colour display[2]. To date, diverse blue-emissive materials have been developed, such as persistent luminescent materials with long-lived emissive lifetimes[6], organic phosphorescent complexes with nearly 100% utilization of both singlet and triplet excitons[7] and purely organic luminogens with thermally activated delayed fluorescence[8]. Recently, organic phosphorescent materials have been developed as alternatives to inorganic persistent luminescent materials through crystallization-inducement[9–11], H-aggregation[12,13], cocrystallization[14,15], polymerization[16,17] or host–guest doping[18,19], as well as many other methods[20–22]. Despite success in achieving tunable emission colours, it remains a formidable challenge to develop heavy-atom-free, blue phosphorescent materials with long lifetimes and high conversion efficiencies.

To obtain phosphorescence in heavy-atom-free organics, two prerequisites are essential: one is to boost triplet excitons by accelerating exciton intersystem crossing (ISC) from singlet- to triplet-excited states; the other is to minimize dissipation of triplet excitons through non-radiative transition by constructing a rigid molecular environment[23–25]. Triplet excitons are known to dissipate through non-radiative transition, delayed fluorescence, triplet–triplet annihilation and luminescence quenching[8,25–29] (Fig. 1a). Crystal engineering through intermolecular locking can promote phosphorescence by suppressing molecular-motion-induced non-radiative transition[30]. However, crystal engineering may dissipate triplet excitons through triplet–triplet annihilation and cause a bathochromic shift in phosphorescence, making it challenging to develop long-lived blue emitters (Supplementary Fig. 2). Notably, phosphorescence emission can blue-shift in a single-molecule state but not in its aggregated state[31]. Furthermore, high-efficiency phosphorescence can be obtained for luminogens in the single-molecule state at 77 K. We reasoned that confining isolated chromophores in rigid crystals with minimal non-radiative transition might notably boost blue phosphorescence efficiency (Fig. 1c).

To validate our hypothesis, we chose pyromellitic acid (PMA) with four carboxyl groups as a model chromophore (Supplementary Scheme 1). These carboxyl groups can ionize in the presence of sodium hydroxide to form multiple ionic bonds and ultimately a rigid molecular network, efficiently suppressing molecular-vibration-induced non-radiative transition. Moreover, exciton ISC in the rigid molecular network can be facilitated to enhance phosphorescence. As a proof of concept, tetrasodium pyromellitate (TSP) was synthesized (Fig. 2a) by volatilizing an aqueous mixture of PMA and NaOH reagents at 323 K. The chemical structure of TSP was characterized by single-crystal X-ray diffraction. The phase purity of TSP crystals was also confirmed by X-ray powder diffraction (Supplementary Fig. 3). Bright deep-blue afterglow

[1]Key Laboratory of Flexible Electronics and Institute of Advanced Materials, Nanjing Tech University, Nanjing, China. [2]Department of Materials Chemistry, Huzhou University, Huzhou, China. [3]State Key Laboratory for Organic Electronics and Information Displays and Institute of Advanced Materials, Nanjing University of Posts and Telecommunications, Nanjing, China. [4]Pharmaceutical, Analytical, and Solid-State Chemistry Research Center, Shanghai Institute of Materia Medica, Chinese Academy of Sciences, Shanghai, China. [5]Department of Chemistry, National University of Singapore, Singapore, Singapore. [6]Joint School of National University of Singapore and Tianjin University, International Campus of Tianjin University, Fuzhou, China. [7]Frontiers Science Center for Flexible Electronics, Xi'an Institute of Flexible Electronics and Xi'an Institute of Biomedical Materials and Engineering, Northwestern Polytechnical University, Xi'an, China. [8]These authors contributed equally: Wenpeng Ye, Huili Ma, Huifang Shi. ✉e-mail: iamzfan@njtech.edu.cn; chmlx@nus.edu.sg; iamwhuang@njtech.edu.cn

was observed for several seconds by the unaided eye after cessation of 310 nm lamp excitation (Supplementary Video 1). Moreover, these organic phosphors showed good chemical and environmental stability, as confirmed by photoluminescence (PL) characterizations under varying conditions (Supplementary Figs. 4–6).

We next investigated the photophysical properties of TSP phosphors under ambient conditions. Both steady-state PL and phosphorescence spectra of TSP crystals showed blue emission at 447 nm (Fig. 2b and Supplementary Fig. 7). The maximal emission lifetime of TSP crystals at 447 nm is 168.39 ms under ambient conditions (Fig. 2c). The phosphorescence nature was further confirmed by a controlled experiment on oxygen sensitivity (Supplementary Fig. 8). The emission band at around 325 nm is indicative of a fluorescence feature with a 0.41 ns lifetime (Supplementary Fig. 9). Both PL and phosphorescence spectra showed dominant emission bands at approximately 447 nm under excitation from 220 to 340 nm (Fig. 2d,e). The absolute phosphorescence quantum efficiency of TSP crystals reached 66.9%. Notably, there was a slight change in both PL and phosphorescence spectra as well as in emission decay at 77 K (Supplementary Figs. 10 and 11). The phosphorescence lifetime of the emission at 447 nm is 209.85 ms (77 K). These results suggest that chromophore ionization can suppress molecular motion for enhanced phosphorescence with the same effect as the low temperature (77 K).

We further conducted a set of experiments in dilute solution and single-crystal states. The phosphorescent spectrum of PMA in dilute solution revealed a dominant emission band at 442 nm (Fig. 3a). After sodium ionization, a similar emission at 447 nm was observed for PMA under the same conditions (Supplementary Fig. 12), indicating that sodium ions did not influence phosphorescence. We speculate that TSP phosphorescence of chromophores in ionic crystals and dilute solution may behave similarly at 77 K. Analysis of molecular distribution in the crystal indicates that PMA chromophores were separated by sodium cations, resembling a cage shape (Fig. 3b,c). Despite a lack of intermolecular interactions between chromophores, each chromophore unit is toggled with numerous chemical bonds, O···O–Na interactions (μ–O, 2.717–2.930 Å, where μ–O represents the oxygen atoms connected to counter ions through ionic bonds) and some water molecules (Supplementary Fig. 17), forming a rigid and isolated molecular environment surrounding the chromophore.

We further confirmed the origin of blue phosphorescence from discrete chromophores rather than chromophore aggregates. Disodium pyromellitate (DSP) was synthesized as a control by changing the molar ratio of PMA/NaOH to 1:2. DSP crystals showed persistent yellow luminescence, lasting approximately 4 seconds upon cessation of the excitation. The PL and phosphorescence emissions of DSP were localized at 391 and 530 nm with lifetimes of 0.41 ns and 354.64 ms, respectively (Fig. 3d and Supplementary Fig. 13). Compared with TSP phosphors, both PL and phosphorescent spectra of DSP only partially overlapped, suggesting a low phosphorescence efficiency (only 2.8% for phosphorescence). Single-crystal analysis indicates that apart from multiple ionic bonding, π–π stacking exists in the aggregated state between phenyl chromophores. Efficient π-orbital coupling between neighbouring phenyl chromophores can suppress non-radiative transitions and enhance phosphorescence (Fig. 3e and Supplementary Figs. 13 and 15). However, compared with TSP, DSP features stronger orbital coupling due to π–π stacking, enabling dissipation of triplet excitons through triplet–triplet annihilation with low phosphorescence efficiency (Supplementary Fig. 16).

We performed theoretical simulations to confirm the influence of ionization on phosphorescence. Upon ionization, the spin–orbit coupling matrix elements increased (Supplementary Fig. 23), consistent with the experimental rate of ISC. The ISC rate ($1.63\times10^{9}\,s^{-1}$) of TSP is 27-fold faster than that of PMA ($6.05\times10^{7}\,s^{-1}$; Supplementary Table 4). Based on experimental and theoretical results, we reasoned that high-efficiency blue phosphorescence derives from the chromophore in a single-molecule state. Strong ionic bonds render each chromophore with a rigid, isolated environment, thereby decreasing non-radiative decay rates and boosting ISC rates (Fig. 3f).

To prove the universality of our approach for high-efficiency blue phosphorescence, we synthesized a series of ionic phosphors with diverse counterions and molecular architectures, including tetrapotassium pyromellitate (TPP), hexasodium mellitate (HSM), hexapotassium mellitate (HPM), tetraammonium pyromellitate (TNP) and tetrabenzylamine pyromellitate (TMP; Fig. 4a and Supplementary Fig. 28). All these phosphors exhibited blue phosphorescence similar to that of the TSP phosphor (Supplementary Fig. 7). Both steady-state PL and phosphorescence spectra exhibited emission peaks at 420, 407, 410, 454 and 464 nm for TPP, HSM, HPM, TNP and TMP crystals, respectively. Notably, the TNP crystal has an absolute quantum efficiency of 96.5% (Fig. 4c). Moreover, we found that all phosphors under study have relatively

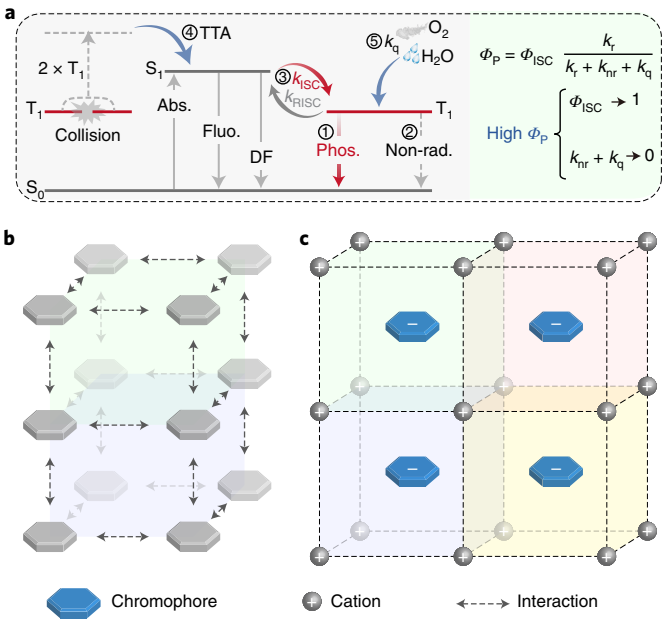

Fig. 1 | Rational design of high-efficiency blue phosphorescence. **a**, Various energy dissipation paths of triplet excitons (left). Note that phosphorescence (phos.) arises from radiative transition (①), while triplet-exciton dissipation is dominated by non-radiative (non-rad.) transition (②). Reverse ISC (③) can also dissipate triplet excitons to produce delayed fluorescence (DF). Additionally, triplet–triplet annihilation (TTA; ④) and luminescence quenching (⑤) by oxygen and water molecules can dissipate triplet excitons. k_r and k_{nr} represent the rate constants of radiative and non-radiative transitions, respectively, from the lowest triplet-excited state (T_1); k_q is the rate constant of triplet-exciton quenching through interactions with surrounding molecules; k_{ISC} is the rate of ISC; k_{RISC} is the rate of reverse ISC; Φ_{ISC} is the efficiency of ISC; Φ_P is the absolute phosphorescence quantum efficiency; S_0 is the ground state; and S_1 is the lowest singlet-excited state. Abs., absorption; fluo., fluorescence. **b**, Conventional molecular stacking in an inefficient phosphorescent crystal shows that weak intermolecular interactions exist through π–π stacking and hydrogen bonding. **c**, Confining an isolated chromophore through ionic bonding for enhanced room-temperature phosphorescence.

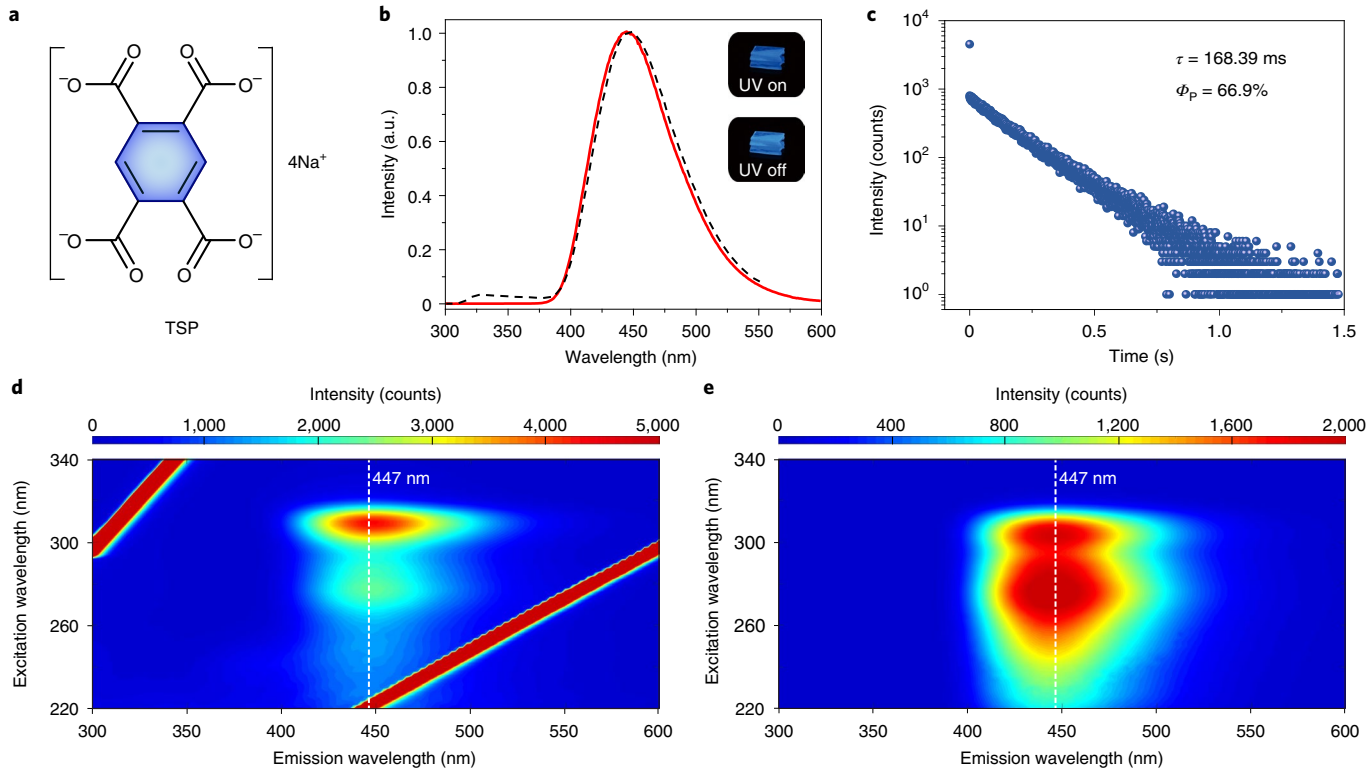

Fig. 2 | Photophysical characterizations of TSP crystals under ambient conditions. a, Chemical structure model of TSP. **b**, Normalized steady-state PL (dashed black line) and phosphorescence (solid red line) spectra, recorded upon excitation at 280 nm. Inset: photographs of the TSP crystal, recorded upon switching on (top) and off (bottom) a 310 nm UV lamp. **c**, Lifetime decay profile of the phosphorescence emission at ~447 nm. τ is the phosphorescence lifetime. **d**, Excitation-PLPL mapping of the TSP crystal (no delay). **e**, Excitation-phosphorescence mapping of the TSP crystal (a delay of 8 ms). The colour change from red to blue in **d** and **e** indicates a decrease in emission intensity.

long lifetimes (101.20–199.17 ms; Fig. 4b,d and Supplementary Fig. 28). Their PL and phosphorescence spectra at 77 K as well as their phosphorescent lifetimes are similar to those obtained at room temperature (Supplementary Figs. 10 and 11), indicating that chromophore ionization and low-temperature treatment have a similar effect on phosphorescence enhancement. As with the TSP phosphor, these ionic phosphors displayed phosphorescence spectra similar to those obtained in dilute solution at 77 K (Supplementary Fig. 12). Analysis of molecular distribution in crystals reveals that these chromophores are arranged in a rigid, isolated environment with high-density ionic bonds (Fig. 4e–h and Supplementary Figs. 18–20 and 28). Chromophore ionization accelerates ISC and boosts triplet-exciton formation (Supplementary Table 4), thus enhancing phosphorescence. Apart from blue phosphorescence, the generality of the strategy of confining isolated chromophores for efficient phosphorescence with different emission colours was further proved in a series of highly conjugated chromophores. A variation from biphenyl and 2,2′-bipyridine to naphthyl derivative changed the phosphorescence colour from green to yellow (Supplementary Figs. 29–31).

We next demonstrated the potential of these phosphors for information encryption and decryption by combining an inkjet-printing technique (Fig. 5a). The letters of the word 'Materials' were encrypted within a sentence, which cannot be discerned by the naked eye under daylight or ultraviolet (UV) irradiation due to background fluorescence (Fig. 5b,c and Supplementary Fig. 32). After excitation with a 310 nm UV lamp, encrypted information appeared in the form of long-lived blue phosphorescence. The recorded information was easily erased within 10 seconds by a purging hydrochloric acid vapour. Moreover, a series of quick-response codes with afterglow features were printed as carriers for data transformation and transfer (Supplementary Fig. 33). After switching off the UV light, quick-response codes gradually appeared. The encrypted website homepage was conveniently identified by scanning the quick-response codes with a handphone (Supplementary Video 2). The application of afterglow phosphors can be extended to fingerprint identification (Fig. 5d and Supplementary Fig. 34).

Beyond the above applications, the afterglow display of phosphors can be combined with electrical excitation. First, a display screen was prepared using grounded TSP powder and ethoxyline resin (Fig. 5e). Homogeneous afterglow was observed after stoppage of UV irradiation, even after immersion of the display screen in water for two weeks (Supplementary Fig. 35). Using a circuit diagram, a photoelectric device of the afterglow display was fabricated (Supplementary Figs. 36–38). Both steady-state and afterglow emission spectra electrically excited are consistent with those under UV excitation (Supplementary Figs. 39 and 40). Numbers from 0 to 9 can be displayed and converted (Fig. 5f and Supplementary Video 3) by manipulating the direct current (Supplementary Table 10). Paths from A to B can be captured under afterglow emission guidance upon ceasing electrical excitation (Fig. 5g, Supplementary Table 11 and Supplementary Video 4). Moreover, based on afterglow display, a demo of a radar scan is achievable under different scan frequencies (Fig. 5h, Supplementary Table 12 and Supplementary Video 5). The scan path was identified within 0.5 s, demonstrating the potential of these phosphors for fast positioning and accuracy tracking.

In summary, we have developed a strategy using confining isolated chromophores for achieving high-efficiency blue or

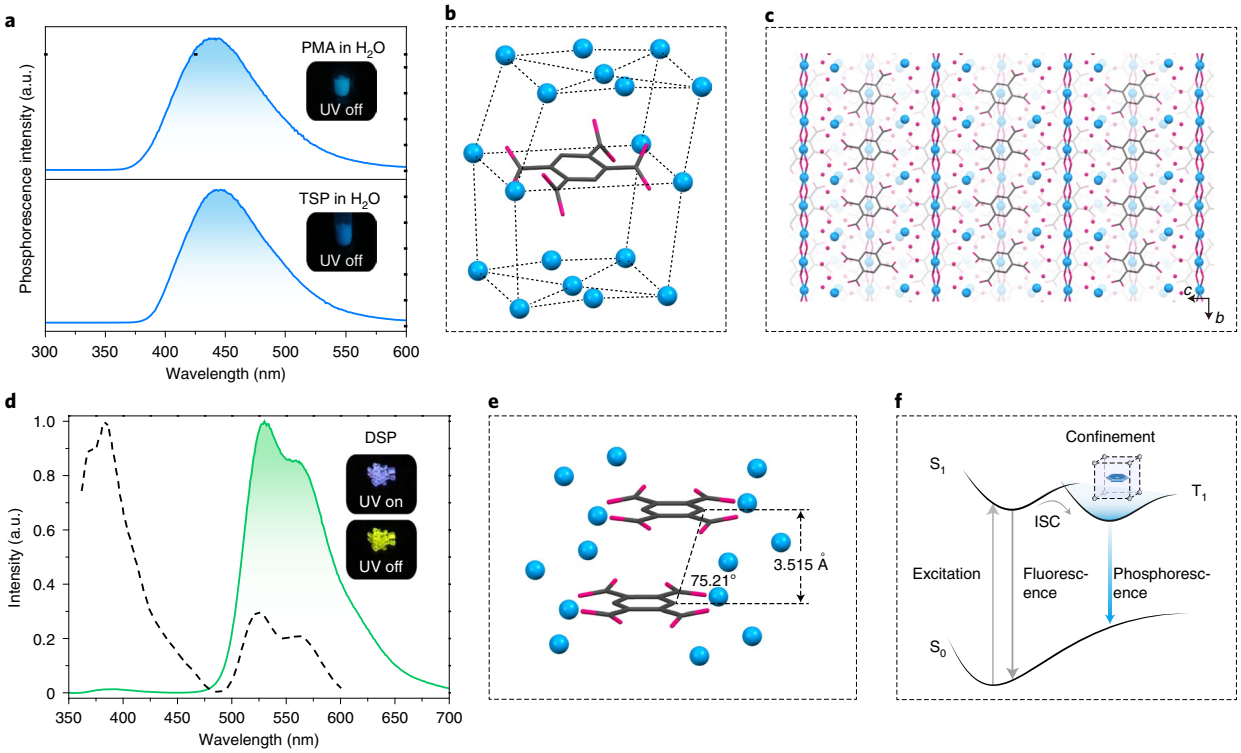

Fig. 3 | Mechanistic investigations of blue phosphorescence under ambient conditions. a, Phosphorescence spectra of PMA and TSP, recorded in dilute solution at 77 K. Inset: photographs of PMA and TSP in H_2O at 77 K after cessation of the excitation at 310 nm. **b**, Schematic of a discrete chromophore (pyromellitic ion) in an ionic crystal. The chromophore is dragged by sodium cations due to ionic bonding, forming an isolated molecular environment. Hydrogen atoms, cocrystallized water molecules and Na–O bonds of the structure are omitted for clarity. Coloured elements: dark grey (C), pink (O) and blue (Na). **c**, Intermolecular stacking viewed along the *a* axis. Hydrogen atoms and Na–O bonds of the structure are omitted for clarity. Coloured elements: dark grey (C), pink (O) and blue (Na). **d**, Normalized steady-state PL (dashed black line) and phosphorescence spectra (solid green line) of the DSP crystal, recorded upon excitation at 340 nm. Inset: photographs of the DSP crystal, recorded upon switching on (top) and off (bottom) a 365 nm lamp. **e**, Molecular packing of the dimer showing a distance of 3.515 Å between intermolecular planes. Coloured elements: dark grey (C), pink (O) and blue (Na). **f**, Proposed energy transfer processes of fluorescence and chromophore-confined phosphorescence.

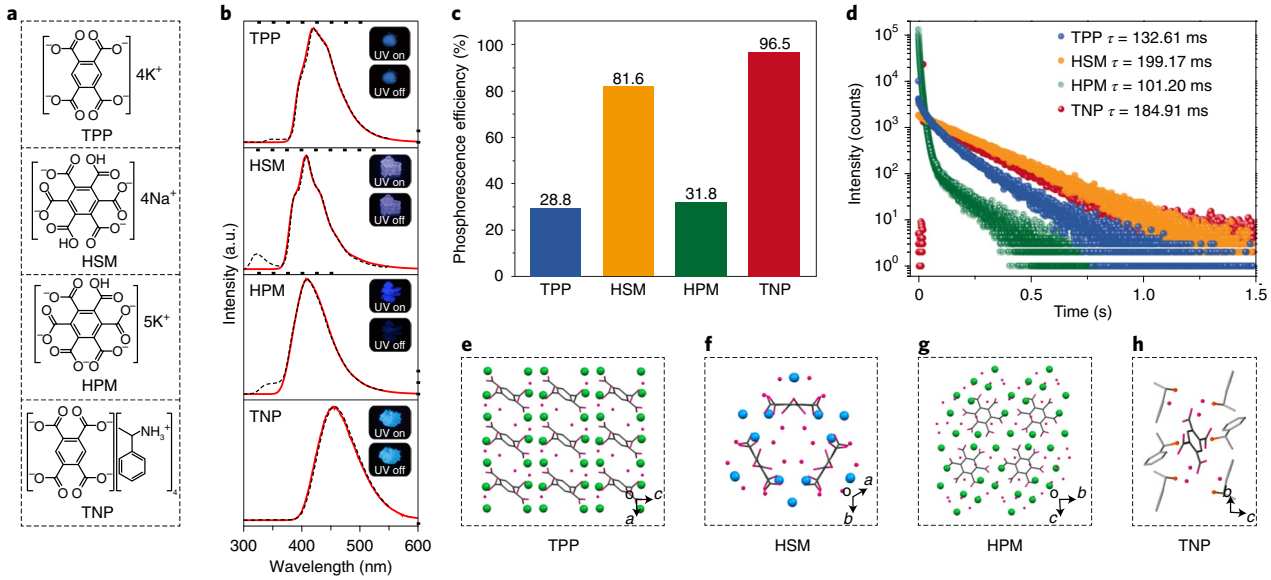

Fig. 4 | Photophysical characterizations of TPP, HSM, HPM and TNP crystals under ambient conditions. a, Chemical structures of TPP, HSM, HPM and TNP. **b**, Normalized steady-state PL (dashed black line) and phosphorescence (solid red line) spectra of the phosphors, recorded upon excitation at 280 nm. Inset: photographs of the phosphors after switching on (top) and off (bottom) a 310 nm UV lamp. **c**, Measured phosphorescence efficiencies of the phosphors. **d**, Lifetime decay profiles of phosphorescence emission at 420, 407, 410 and 454 nm for TPP, HSM, HPM and TNP phosphors, respectively. **e**–**h**, Molecular stacking of TPP, HSM, HPM or TNP, respectively, in the crystal. Hydrogen atoms, Na–O and K–O bonds of these structures are omitted for clarity. Coloured elements: dark/light grey (C), pink (O), green (K), dark blue (Na) and orange (N).

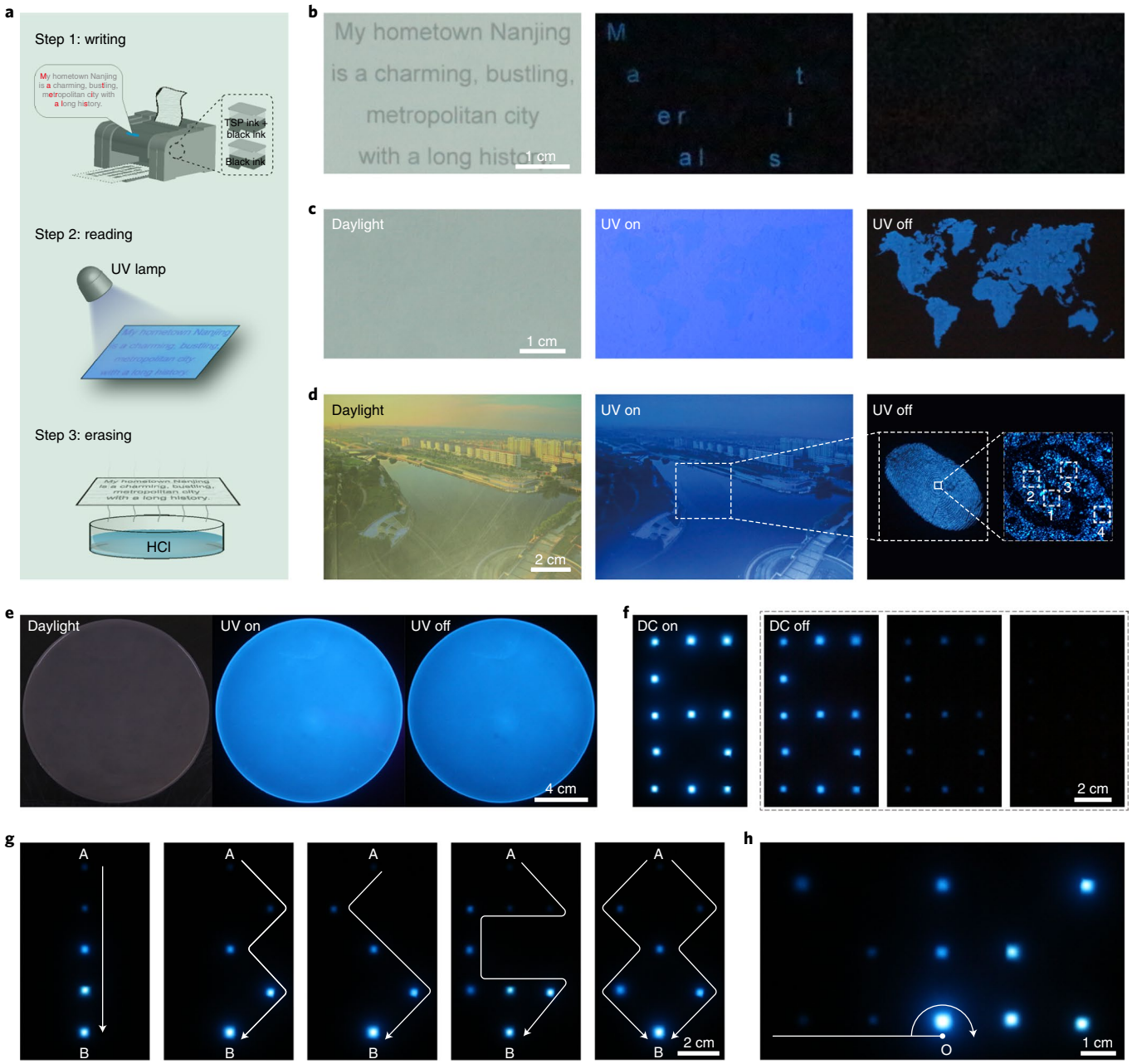

Fig. 5 | Demonstration of blue phosphorescence for data encryption, fingerprint identification and afterglow display under ambient conditions. a, Schematic of inkjet-printing encryption of TSP inks used to create writing, reading and erasing operations. **b**, Photographs of a sentence for information encryption under daylight (left panel) or UV light off (middle panel). Note that the encrypted information can be quickly erased with HCl vapour (right panel). **c**, Images of a world map inkjet printed with the TSP ink. **d**, Photographs of a fingerprinted painting taken under daylight (left panel) or UV light on–off switching (middle and right panels). Close-up: numbers 1 to 4 show different sweat pores of the fingerprint. **e**, Photographs of a display screen taken under daylight (left panel) or UV light on–off switching (middle and right panels). **f**, Digit display under direct current (DC) switched on and off, with time passing from left to right in the three 'off' panels. **g**, Afterglow display of different paths from A to B by controlling direct current on and off. **h**, Demonstration of radar scan mimicry (scan time, 0.5 s).

deep-blue phosphorescence. Chromophore ionization enables a 96.5% phosphorescence efficiency and a 184.91 ms triplet lifetime. Our experimental data indicate that counterions have great utility in enhancing phosphorescence efficiency in the solid state. High-density ionic bonding to chromophores suppresses non-radiative transition and facilitates exciton generation, thereby boosting phosphorescence efficiency. This study may pave the way towards high-performance organic phosphors for broad future applications from display and lighting to data encryption and bioimaging.

Online content

Any methods, additional references, Nature Research reporting summaries, source data, extended data, supplementary information, acknowledgements, peer review information; details of author contributions and competing interests; and statements of data and code availability are available at https://doi.org/10.1038/s41563-021-01073-5.

Received: 15 October 2019; Accepted: 5 July 2021;
Published online: 23 August 2021

References

1. Xu, H. et al. Recent progress in metal–organic complexes for optoelectronic applications. *Chem. Soc. Rev.* **43**, 3259–3302 (2014).
2. Pan, M., Liao, W., Yin, S., Sun, S. & Su, C. Single-phase white-light-emitting and photoluminescent color-tuning coordination assemblies. *Chem. Rev.* **118**, 8889–8935 (2018).
3. Zhang, K. et al. Long-lived emissive probes for time-resolved photoluminescence bioimaging and biosensing. *Chem. Rev.* **118**, 1770–1839 (2018).
4. Deng, W. et al. 2D Ruddlesden–Popper perovskite nanoplate based deep-blue light-emitting diodes for light communication. *Adv. Funct. Mater.* **29**, 1903861–1903869 (2019).
5. Nanishi, Y. The birth of the blue LED. *Nat. Photon.* **8**, 884–886 (2014).
6. Li, Y., Gecevicius, M. & Qiu, J. Long persistent phosphors—from fundamentals to applications. *Chem. Soc. Rev.* **45**, 2090–2136 (2016).
7. Baldo, M. et al. Highly efficient phosphorescent emission from organic electroluminescent devices. *Nature* **395**, 151–154 (1998).
8. Hirata, S. et al. Highly efficient blue electroluminescence based on thermally activated delayed fluorescence. *Nat. Mater.* **14**, 330–336 (2015).
9. Yang, J. et al. The influence of the molecular packing on the room temperature phosphorescence of purely organic luminogens. *Nat. Commun.* **9**, 840 (2018).
10. Shoji, Y. et al. Unveiling a new aspect of simple arylboronic esters: long-lived room-temperature phosphorescence from heavy-atom-free molecules. *J. Am. Chem. Soc.* **139**, 2728–2733 (2017).
11. Yang, Z. et al. Intermolecular electronic coupling of organic units for efficient persistent room-temperature phosphorescence. *Angew. Chem. Int. Ed.* **55**, 2181–2185 (2016).
12. An, Z. et al. Stabilizing triplet excited states for ultralong organic phosphorescence. *Nat. Mater.* **14**, 685–690 (2015).
13. Lucenti, E. et al. Cyclic triimidazole derivatives: intriguing examples of multiple emissions and ultralong phosphorescence at room temperature. *Angew. Chem. Int. Ed.* **56**, 16302–16307 (2017).
14. Bolton, O., Lee, K., Kim, H., Lin, K. & Kim, J. Activating efficient phosphorescence from purely organic materials by crystal design. *Nat. Chem.* **3**, 205–210 (2011).
15. Wei, J. et al. Induction of strong long-lived room-temperature phosphorescence of *N*-phenyl-2-naphthylamine molecules by confinement in a crystalline dibromobiphenyl matrix. *Angew. Chem. Int. Ed.* **55**, 15589–15593 (2016).
16. Ma, X., Xu, C., Wang, J. & Tian, H. Amorphous pure organic polymers for heavy-atom-free efficient room-temperature phosphorescence emission. *Angew. Chem. Int. Ed.* **57**, 10854–10858 (2018).
17. Cai, S. et al. Enabling long-lived organic room temperature phosphorescence in polymers by subunit interlocking. *Nat. Commun.* **10**, 4247 (2019).
18. Kabe, R. & Adachi, C. Organic long persistent luminescence. *Nature* **550**, 384–387 (2017).
19. Su, Y. et al. Ultralong room temperature phosphorescence from amorphous organic materials toward confidential information encryption and decryption. *Sci. Adv.* **4**, 9732–9743 (2018).
20. Zhang, G., Palmer, G., Dewhirst, M. & Fraser, C. A dual-emissive-materials design concept enables tumour hypoxia imaging. *Nat. Mater.* **8**, 747–751 (2009).
21. Gao, R., Mei, X., Yan, D., Liang, R. & Wei, M. Nano-photosensitizer based on layered double hydroxide and isophthalic acid for singlet oxygenation and photodynamic therapy. *Nat. Commun.* **9**, 2798 (2018).
22. He, Z. et al. Achieving persistent, efficient, and robust room-temperature phosphorescence from pure organics for versatile applications. *Adv. Mater.* **31**, 1807222 (2019).
23. Hirata, S. Recent advances in materials with room-temperature phosphorescence: photophysics for triplet exciton stabilization. *Adv. Optical Mater.* **5**, 1700116 (2017).
24. Kenry, C. C. & Liu, B. Enhancing the performance of pure organic room-temperature phosphorescent luminophores. *Nat. Commun.* **10**, 2111 (2019).
25. Baryshnikov, G., Minaev, B. & Agren, H. Theory and calculation of the phosphorescence phenomenon. *Chem. Rev.* **117**, 6500–6537 (2017).
26. Kwon, M. et al. Suppressing molecular motions for enhanced room-temperature phosphorescence of metal-free organic materials. *Nat. Commun.* **6**, 8947 (2015).
27. Sternlicht, H., Nieman, G. & Robinson, G. Triplet–triplet annihilation and delayed fluorescence in molecular aggregates. *J. Chem. Phys.* **38**, 1326–1335 (1963).
28. Schulman, E. & Parker, R. Room temperature phosphorescence of organic compounds. The effects of moisture, oxygen, and the nature of the support-phosphor interaction. *J. Phys. Chem.* **81**, 1932–1939 (1977).
29. Schulman, E. & Walling, C. Phosphorescence of adsorbed ionic organic molecules at room temperature. *Science* **178**, 53–54 (1972).
30. Braga, D., Grepioni, F. & Desiraju, G. Crystal engineering and organometallic architecture. *Chem. Rev.* **98**, 1375–1405 (1998).
31. Gu, L. et al. Colour-tunable ultra-long organic phosphorescence of a single-component molecular crystal. *Nat. Photon.* **13**, 406–411 (2019).

Methods

General procedure for the synthesis of phosphors. *TSP.* PMA (0.254 g, 1.0 mmol), NaOH (0.160 g, 4.0 mmol) and deionized water (5.0 ml) were added into a polypropylene (PP) centrifugal tube, forming a transparent solution. Then the water was evaporated by heating at 50 °C (oil bath), leaving block colourless crystals (0.205 g, 37.5%) in the tube.

DSP. The synthesis of DSP was similar to that of TSP except for changing the molar ratio of PMA/NaOH to 1:2. Colourless crystals were obtained in 56.1% yield (0.184 g).

TPP. The synthesis of TPP was similar to that of TSP except that NaOH was replaced by KOH. Colourless crystals were obtained in 53.9% yield (0.258 g).

HSM. Mellitic acid (0.085 g, 0.249 mmol), NaOH (0.060 g, 1.494 mmol) and deionized water (2.0 ml) were added into a PP centrifugal tube, forming a transparent solution. Then the water was evaporated by heating at 50 °C, leaving block colourless crystals (0.093 g, 58.9%) in the tube.

HPM. The synthesis of HPM was similar to that of HSM except that NaOH was replaced by KOH, affording colourless crystals (0.078 g, 49.9%).

TNP. The synthesis of TNP was similar to that of TSP except that NaOH was replaced by alpha-methylbenzylamine. Colourless crystals were obtained in 47.6% yield (0.403 g).

Procedure of inkjet printing. PMA (2.54 g, 10.0 mmol), NaOH (1.6 g, 40.0 mmol) and deionized water (10.0 ml) were added to a PP centrifugal tube to prepare TSP inks. The solution was heated to dissolve the solute completely. After the solution was cooled to room temperature, TSP crystals precipitated at the bottom of the tube, and the top, saturated solution was the TSP ink. An inkjet printer was used to print TSP molecules for information encryption and decryption. Information can be printed on paper using two inks that are prepared by adding an equal amount of the TSP ink or deionized water into a black ink. Following excitation using a 310 nm UV lamp, encrypted information was decoded through long-lived blue phosphorescence. The decoded information can be re-encrypted by exposing to hydrochloric acid for 10 seconds.

Fabrication of afterglow films for display. TSP crystals were first grounded for 15 min. Then TSP powder (0.5 g) and ethoxyline resin (15 g) were added to a beaker and stirred for 30 min. After that, a curing agent (5 g) was added and stirred for another 5 min. The mixture was put into a mould and left standing for 24 h, affording a homogeneous film.

Data availability

Source data are provided with this paper. The remaining data supporting the findings of this study are available within the paper and its Supplementary Information files and are available from the corresponding authors upon reasonable request.

The X-ray crystallographic coordinates for structures reported in this study have been deposited at the Cambridge Crystallographic Data Centre under deposition numbers 1888289, 1888291–1888293, 2011667–2011675, 2015867 and 2024673. These data can be obtained free of charge from the Cambridge Crystallographic Data Centre via www.ccdc.cam.ac.uk/data_request/cif.

Acknowledgements

This work is supported by the National Key R&D Program of China (2020YFA0709900), the National Natural Science Foundation of China (21875104, 21975120, 51673095, 21973043, 91833304 and 91833302), the Natural Science Fund for Distinguished Young Scholars of Jiangsu Province (BK20180037) and the Postgraduate Research & Practice Innovation Program of Jiangsu Province (KYCX21_1098). We are grateful to the High-Performance Computing Center of Nanjing Tech University for technical support.

Author contributions

W. Ye, H.S., H.M., Z.A., X.L. and W.H. conceived the experiments and wrote the paper. W. Ye, H.W., L.B., C.M., W.J., J.Z., J.L., Z.S. and X.H. were primarily responsible for the experiments. S.C., S.L., C.D. and H.Z. performed the lifetime measurements. K. Ling, M.Z., W. Yao, Z.Z. and K.S. conducted the single-crystal measurement and analysis. X.Y., Yanyun Zhang, K. Liu and Yujian Zhang measured the quantum efficiency. A.L., M.G. and H.M. contributed to the time-dependent density functional theory calculations. C.G., Y.M. and Y. Zhou programmed the codes for applications. All authors contributed to data analyses.

Competing interests

The authors declare no competing interests.

Additional information

Supplementary information The online version contains supplementary material available at https://doi.org/10.1038/s41563-021-01073-5.

Correspondence and requests for materials should be addressed to Z.A., X.L. or W.H.

Peer review information *Nature Materials* thanks Jinsang Kim and the other, anonymous, reviewer(s) for their contribution to the peer review of this work.

Reprints and permissions information is available at www.nature.com/reprints.